almaida.firdaus@cern.ch

Optical Characterization of Aerogel and Anti-Reflection Coating of Silicon Photomultipliers for Ring Imaging Cherenkov Detector

Almaida Firdaus
Supervisor: Antonello Di Mauro
CERN, CH-1211 Geneva, Switzerland

Keywords: Optical Characterization, Aerogel, ARC of SiPM, RICH Detector

Abstract

In the context of the ALICE upgrade system for Run 5, a Ring Imaging Cherenkov (RICH) detector has been proposed to perform charged Particle Identification (PID) in the momentum range 0.5-15 GeV/c. It consists of an Aerogel radiator and a Silicon Photomultipliers (SiPM) array with sensitivity to single photons in the visible range. The performance of particle identification strongly depends on the amount of Cherenkov photons detected by the RICH Detector and is affected by the optical properties of both Aerogel and SiPM. In this paper, the optical characterization of 15 aerogel tiles of 10x10 cm^2 has been performed in the wide spectrum from 250 to 800 nm using an Integrated Sphere (IS) setup. In addition, the reflectivity of Silicon has also been studied, various samples have been prepared using different films in combination with a so-called textured etching, and the reflection properties have been measured using the same setup to identify the optical properties in Anti-Reflection Coating (ARC) of SiPM.

Contents

1 Introduction

1.1 General Overview of ALICE 3 Proposal

A Large Ion Collider Experiment (ALICE) is one of the collaboration experiments in the Large Hadron Collider (LHC) at CERN dedicated to studying Quark-Gluon Plasma (QGP) from heavy-ion collisions. Quark-gluon plasma is a state of matter existing at extremely high temperatures and densities when composite states called hadrons lose their identity and dissolve into a soup of their constituent. This matter is believed to have filled the entire universe shortly after the Big Bang. ALICE program will determine the properties of strongly interacting matter and discern how they arise from the underlying interactions as described by quantum chromodynamics. Collisions of heavy nuclei at the LHC provide unique experimental access to the hottest and longest-lived quark-gluon plasma available in the laboratory with abundant production of heavy flavor probes [10].

A next generation of a heavy-ion experiment called ALICE 3 has been proposed to address the various questions that will be left open by the present ALICE experiment, which will end the operation at Run 4 in 2023. For particle identification on ALICE 3, one of five different detector systems is a Ring Imaging Cherenkov (RICH) Detector that provides particle identification in the momentum range up to 2 GeV/c. The calorimeter would be based on a combination of lead-sampling and lead-tungstate segments, by commercially available Silicon Photomultipliers. In addition, the detection layers of the muons identifier, resistive plate chambers, and scintillating bars are being considered [1].

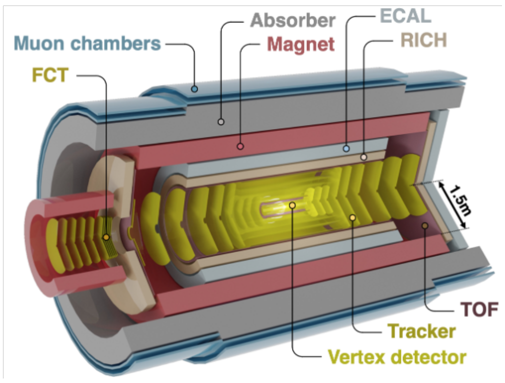

Figure 1: Layout of ALICE 3 Detector[2]

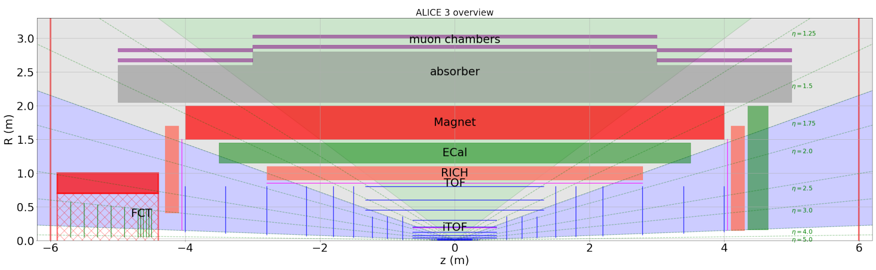

Figure 2: Cross-section layout of ALICE 3 Detector

Figure 1 and 2 show the layout of ALICE 3 Detector proposal. The nearest part to the place where particle collisions happened is a Vertex Detector. Following Inner Tracking System which determines the primary and secondary vertex of the particle decay channels. Next upper the ITS is Time of Flight Detector, the TOF will providing charged particle identification in the momentum range 2 GeV/c. Behind the TOF, the RICH Detector is located at an angular momentum 1.5 mrad for extended particle identification up to 2 GeV/c and 1 GeV/c for electrons and hadrons respectively. This followed by the Electromagnetic Calorimeter which subsequently surrounded by a large superconducting magnet, the absorber layers and the muon chamber [15].

This proposal is especially focusing to RICH detector by studying the aerogel in many various refractive index (n=1.03; 1.04; 1.05; 1.005) as Cherenkov radiator and a layer of Silicon Photomultipliers (SiPM) with textured etching surface by silicon dioxide for the photon detection. Furthermore, We will discus those materials by identified the optical properties (transmittance and reflectance) from the integrated sphere measurements.

2 Theoretical View

2.1 Cherenkov Radiation and its Applications

Cherenkov radiation was first experimentally studied by physicist Pavel Cherenkov in 1934. Cherenkov radiation happened when the charged particles travel through the medium larger than the speed of light in the same medium. Its application is on particle detector called RICH detector. If the charged particles move through an isolator of initially constant refraction index (n), the latter is polarized by the electromagnetic field of the flying particle. Usually this polarization superpose destructively and the perturbation can relax while the particle moves on. But if the speed of the particle β is higher than the phase velocity of light in the medium $C_n = n^{-1}$ the perturbation can no longer decay since the reaction time of the medium is not high enough and the perturbation remains behind the particle. Due to the Huygens principle there occurs a wave front at $\beta > C_n$ but only single spherical waves at $\beta < C_n$. The particle moves along the projection of the red arrow and runs during a time $\boldsymbol{t}$ through a distance $x_T = \beta$.t. In between the Cherenkov radiation travels radially by a distance $X_s = \frac{t}{n}$. Since the wave front represents the tangent on the radiated elementary waves there is a right angle as shown in Figure 3. Using simple trigonometric relations one can determine the Cherenkov angle by this equation.

$$cos(\theta_c) = \frac{1}{\beta_n} \tag{1}$$

Where θ is the opening angle of the cone, $\boldsymbol{n}$ is the refractive index of the medium, and $\beta = \frac{v}{c}$ where v is the velocity of the particle and c is the speed of light [16].

Cherenkov radiation is an another method to identify particles for a higher energy range in the same energy region by measuring the energy ionization loss per unit of track length in a gas. For particle travelling at low velocities, these pulses will cancel each other because of the symmetry. However, when the velocity of the particles is larger, the polarization will be retarded with respect to particles trajectory, resulting in a cone-like coherent electromagnetic wavefront (Cherenkov radiation) [6]. Threshold Cherenkov (TC) counters use the Cherenkov

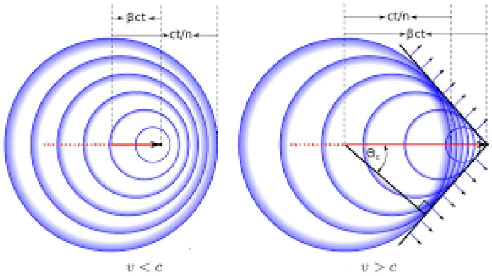

Figure 3: The Cherenkov radiation caused by the charged particle when travel thorugh the medium. An illustration when $\beta < C_n$ [left]; an illustration when $\beta > C_n$ [right]

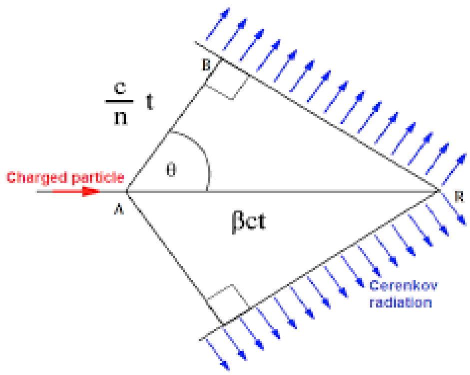

Figure 4: The Cherenkov angles around the moving particle [8]

condition ($\beta n > 1$) to determine whether the velocity of a charged particles are below or above a threshold value [7]. This only allows identification in a small energy range. Ring Imaging Cherenkov (RICH) detector, that measure the Cherenkov angle for charged particles, can be used to identify particles in the energy range of 0 - 100 GeV.

2.2 Ring Imaging Cherenkov (RICH) Detector

Ring Imaging Cherenkov or RICH Detector is one of detector based on the detection of Cherenkov radiation. The photon that is emitted in the radiator can be subsequently focused by a spherical mirror onto a photon detector creating the characteristic ring-like image of photo-electrons. Charged particles which traversing a medium with different momentum can be distinguish by measuring the Cherenkov angle.

The separation of charged particles based on Cherenkov angle can be optimised by choosing the best type of radiation material. The transparent dielectric medium in radiator is effective to use with the refractive index of the material (n) related to the speed of light in a medium $\frac{c}{n}$, also causes minimal scattering and absorption of the photon as well as possible. In case of best material of Cherenkov radiator, the silica-aerogel ($nSiO_2+2nH_20$) has several benefits. Silica aerogel has a net-like structure are kept statically makes it extremely good as insulator and has a low density.

Furthermore, it is required that Cherenkov radiation do not scatter in the medium since the angular dispersion caused by the radiator reduces the precision of the Cherenkov angle. The main background in aerogel is caused by Rayleigh Scattering which is the elastic scattering of the light by particles smaller than the wavelength as $1/\lambda^4$ and causes the blue-ish haze observed in aerogel. Together with the absorption of light in the medium, this result in lower transmission of light through aerogel. Additionally, Mie Scattering can occur, which does not influence the transmittance (T) of the medium. This effect is independent of λ and dependent on the thickness (t) of the aerogel. Mie scattering occurs due to microscopic density fluctuations in the sample and surface of thickness at the boundaries [4].

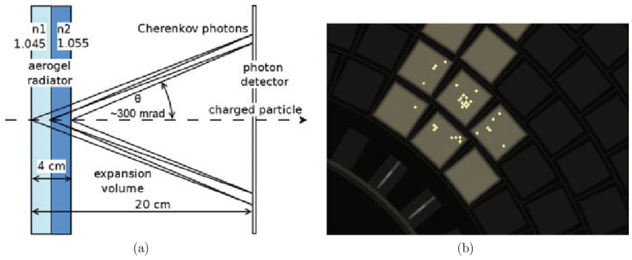

Figure 5: (a) General Set-up of RICH Detector; (b) Particles detected in RICH detector

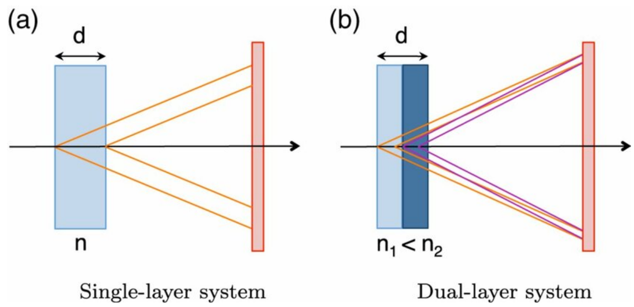

Figure 6: Different possibilities of RICH Detector set-up with single-layer and dual-layer system [9]

As shown in Figure 5, the general set-up of the RICH Detector system installed following the TOF detector is derived from the requirement to extend the e/ϕ separation from 500 MeV/c (TOF limit) to 2 GeV/c and the charged hadron identification (3σ ϕ/K separation) up to 10 GeV/c. Besides aerogel application as Cherenkov radiation, another set-up of RICH Detector is a photo-detection layer 20 cm from the radiator. The performance of SiPMs has been assumed for the photon detector especially a peak Photon Detection Efficiency (PDE) of 40% and a Dark Count Rate (DCR) of 50 $kHzmm^-2$

3 Methodology

3.1 Set-up of Measurement

The measurements of aerogel and silicon were performed using UV/VIS Spectrometer lambda 650 with integrated sphere set-up. For detail measurement set-up of aerogel and silicon can be seen in these figures below.

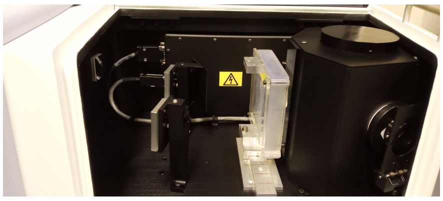

Figure 7: The set-up for aerogel measurement

In addition, the reflectance measurement for silicon was used the same set-up. The sample was putted on the back of spectrometer and removed the reflectance port. The set-up can be seen in Figure 8.

Figure 8: The set-up for silicon measurement

3.2 List of the Samples

The samples of aerogel were produced from Chiba University in Japan. Totally, there are 15 samples which measured in this research. The list of samples are shown in the table 1, together with their thickness and the refractive index (n). The samples can not be touched directly, therefore we use sample holder (10x10 cm^2) and mounted into a metal ridge which allowed to slide perpendicular with the beam (light source). The holder was additionally allowed to move a position upward and make it easier to adjust different position in 15 points.

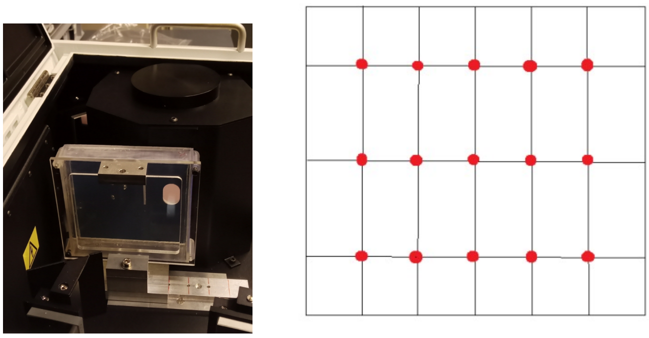

Figure 9: Sample holder and metal ridge in the aerogel set-up (left); 15 sample points (right)

Table 1: List of aerogel samples

Samples	Refractive Index (n)	Thickness (mm)
LEC4-2a	1.03	20.8
LEC4-2b	1.03	20.7
LEC6-1a	1.03	20.1
LEC6-1b	1.03	20.5
LEC6-2b	1.03	20.4
LEC11-6	1.04	20.3
LEC11-7	1.04	20.5
LEC12-1	1.04	20.3
LEC12-4	1.04	20.4
LEC12-6	1.04	20.5
LEC8-1	1.05	20.5
LEC8-2	1.05	20.5
LEC8-6	1.05	20.5
LEC9-1	1.05	20.6
LEC9-2	1.05	20.8

The silicon wafers used in this study are performed with KOH for anisotropic silicon etch process in the volume ratio 3:4 (3% pottasium hydroxide (KOH) alkaline and 4% isopropyl alcohol (IPA)) and deionized (DI) water mixture solutions at a high temperature of 80^0C. After the texturing, the wafers were cleaned in a 5% HF Solution. We used 6 samples of silicon listed in the table below together with their different etching time.

Table 2: List of silicon samples

Samples	Duration of Etching Process
A	Bare silicon
B	4 minutes
C	8 minutes
D	16 minutes
E	20 minutes
F	28 minutes

3.3 The Optical Properties of Aerogel

In this research, the transmittance and the reflectance coefficients were performed to identify the optical properties of aerogel. The transmittance of aerogel is a measure of how much light passes through the material without being absorbed or scattered. The measurements were perfomed at CERN (Reflectometer Laboratory, Building 3/R-022) on July-August 2023 using a Perkin Elmer Lambda 650 Spectrometer. A Deuterium light source was used to cover the UV ligth spectrum in the range from 250-300 nm, and visible light spectrum in the range from 300-800 nm. The spectrometer was taken the result every 5 nm step.

3.3.1 Transmittance Measurement

The transmittances were measured for total and diffused part. As the light traverses the aerogel, it is partially forward scatter, backward scatter and/or absorbed. Since the gap is slightly wider than the light beam, the part of the light can enter the sphere and gets reflected at the inner surface. As a Reference, a beam passed alongside the sample beam without traversing any sample. The integrated sphere allowed for several set-ups which were used for the measurement of transmitted total and diffuse part of the light. The total transmittance was measured while keeping the reflectance port attached to the sphere in order to prevent the beam from escaping the setup. Then, the diffuse part was determined by removing the reflectance port and exclusively detecting the diffuse light component of the beam. Finally, the linear transmittance defined as the difference between total and diffused part. These measurements was obtained from all samples at 15 points. For the total transmittance, the white reflectance port is kept on the integrated sphere. The set-up also used the black tissue on the back to cover a hole in the back and turned off the lights in the laboratory to provide good measurements.

The measurements of 15 point on each samples will provide information on the dependence of the transmittance on the thickness as well as on the light wavelength in the range 250-800 nm. Its dependance on the radiation wavelength can be defined by the Hunt Formula:

$$T(\lambda) = e^{-\frac{t}{\lambda_T}} = A_e^{-\frac{C*t}{\lambda^4}} \tag{2}$$

where C is the aerogel clarity, A represents the coefficient of surface scattering, t is the sample thickness and λ_T is the transmission length. The mapping for transmittance measurements can be seen in Figure 10.

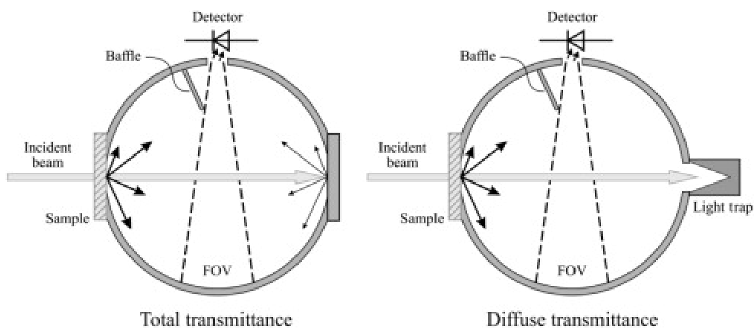

Figure 10: Set-up for total and diffuse for aerogel transmittance measurements[3]

3.3.2 Reflectance Measurement

For reflectivity, the amount of light reflected by the detector was done by replacing the reflectance port with the sample and detecting the light reflected by the aerogel. The reflection values were measured by putting the sample on the back (back scattering) and covered by black tissue and also the lights in the laboratory is off. The reflectance values was measuring for all 15 samples at 3 points in the middle surface using the same general set-up.

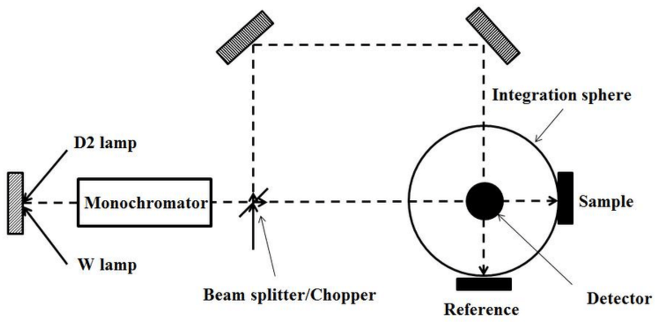

Figure 11: Set-up for aerogel reflectance measurement[13]

3.4 The Optical Properties of Silicon

3.4.1 Reflectance Measurement

For silicon reflectivity, the measurement was done by replacing the reflectance port with the sample as the same measurement for the aerogel. The reflection value is measured by putting the silicon on the back (back scattering) and covered by black tissue and also the lights in the laboratory is off. The reflectance values was measuring for all samples of different duration of etching structured.

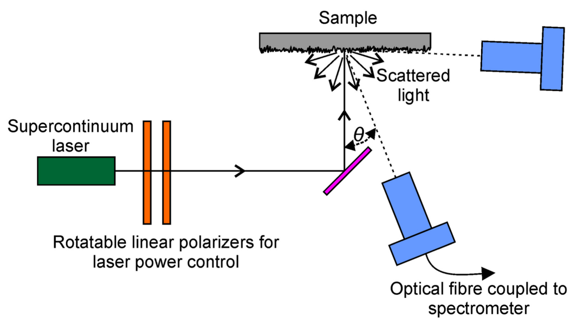

Figure 12: Set up for silicon reflectance measurement [11]

4 Result and Discussion

4.0.1 Total and Diffuse Transmittance of Aerogel (n=1.03)

The %Transmittance was obtained of all samples and displayed in this section. The wavelength are shown in the x-axis and the transmittance values are shown in the y-axis. There are three different types of refractive index used for this measurement, the one with n=1.03; n=1.04 and n=1.05. These plots show the transmittance for total and diffuse part of each samples in 15 points. These lines explain the homogeneous of all surface of the aerogel, once the surface is not really clear it will affect the distribution and the transmittance value as we can see, several tiles not really clean so the line is much higher.

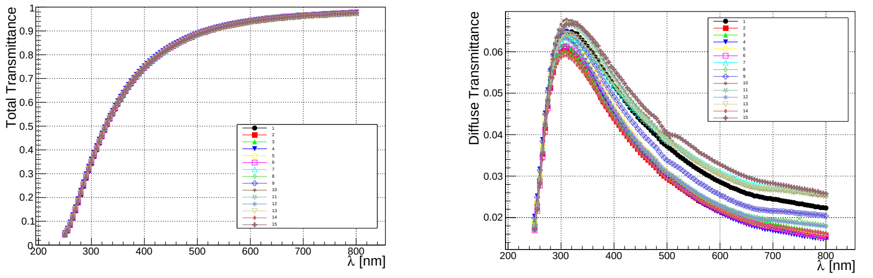

Figure 13: Total and Diffuse Transmittance sample LEC4-2a

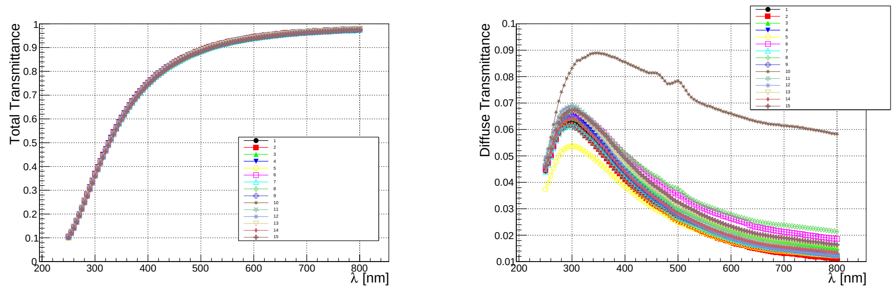

Figure 14: Total and Diffuse Transmittance sample LEC4-2b

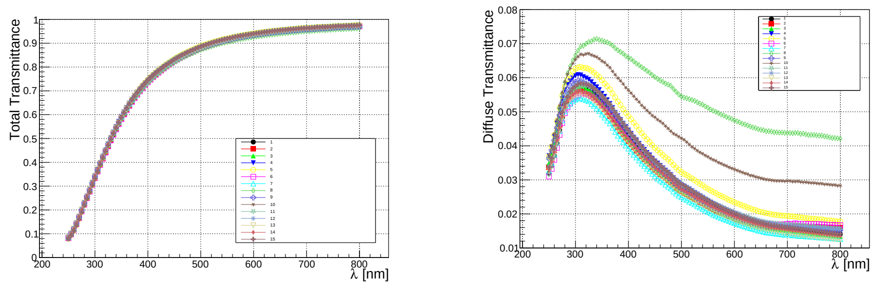

Figure 15: Total and Diffuse Transmittance sample LEC6-1a

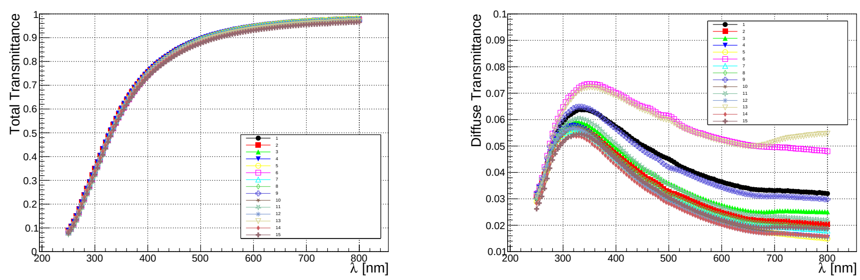

Figure 16: Total and Diffuse Transmittance sample LEC6-1b

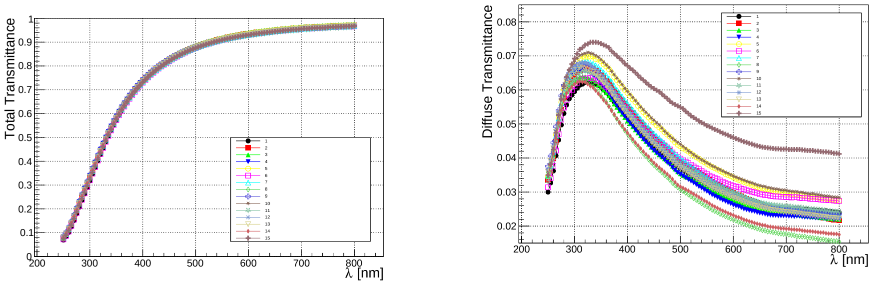

Figure 17: Total and Diffuse Transmittance sample LEC6-2b

4.0.2 Total and Diffuse Transmittance of Aerogel (n=1.04)

The separation of the particles based on the Cherenkov angle can be optimised by choosing the best type of material used for radiator, where the refractive index of the material (n) related to the speed of light in the medium $v = \frac{c}{n}$. furthermore, it is required that the radiator should have maximal transmission of the photon as possible. These figures explain the differences of transmittance values in the refractive index of aerogel n=1.04.

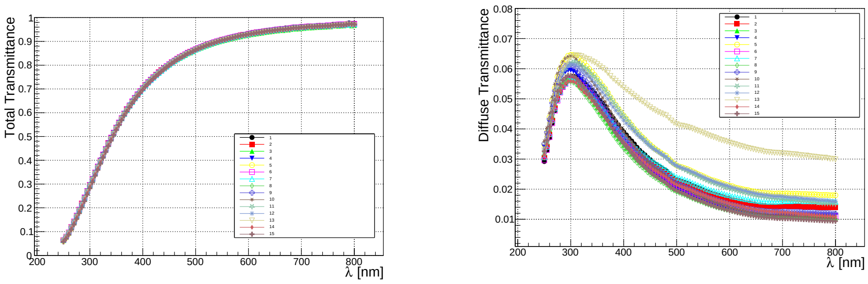

Figure 18: Total and Diffuse Transmittance sample LEC11-6

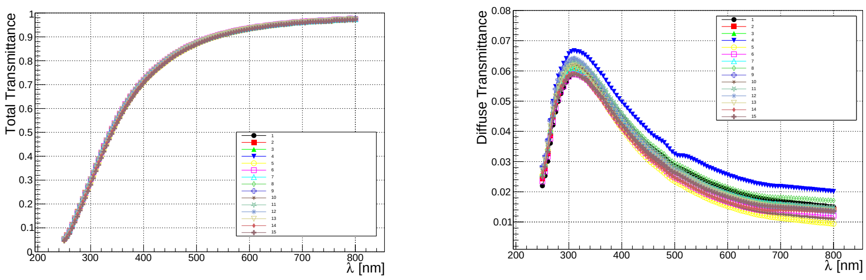

Figure 19: Total and Diffuse Transmittance sample LEC11-7

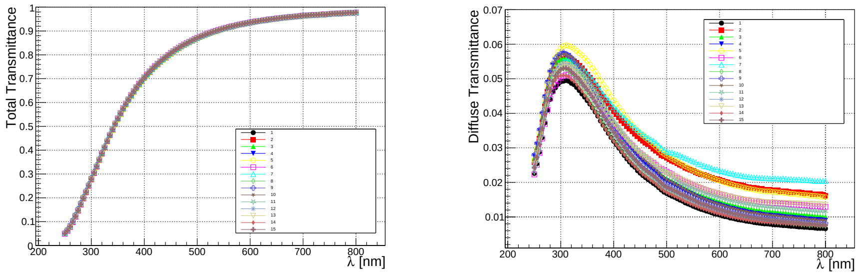

Figure 20: Total and Diffuse Transmittance sample LEC12-1

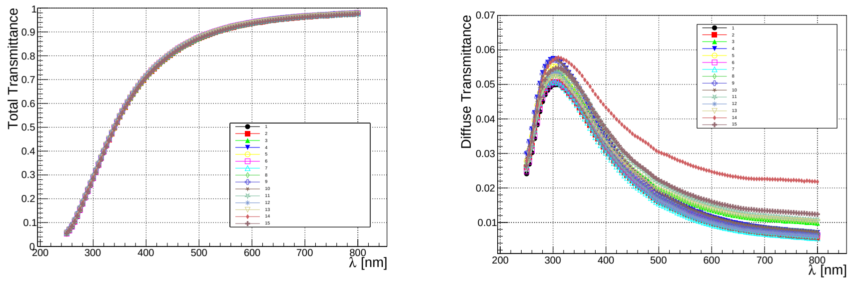

Figure 21: Total and Diffuse Transmittance sample LEC12-4

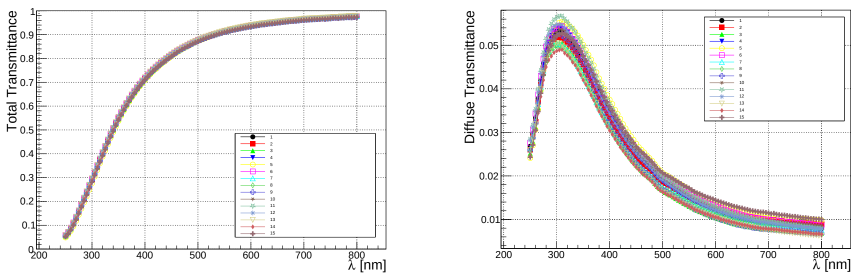

Figure 22: Total and Diffuse Transmittance sample LEC12-6

4.0.3 Transmittance values of Aerogel (n=1.05)

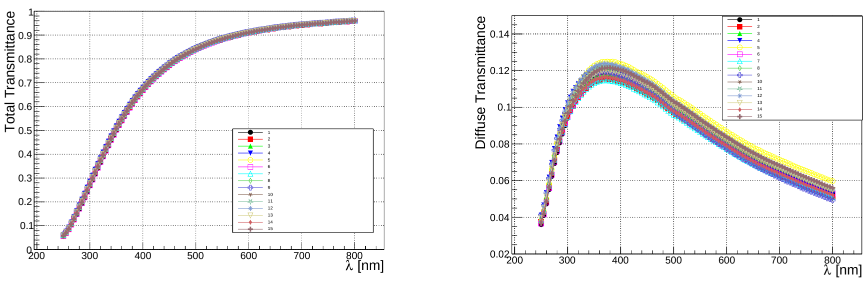

Figure 23: Total and Diffuse Transmittance sample LEC8-1

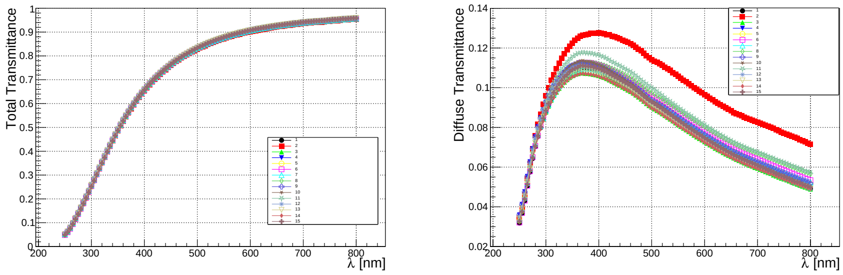

Figure 24: Total and Diffuse Transmittance sample LEC8-2

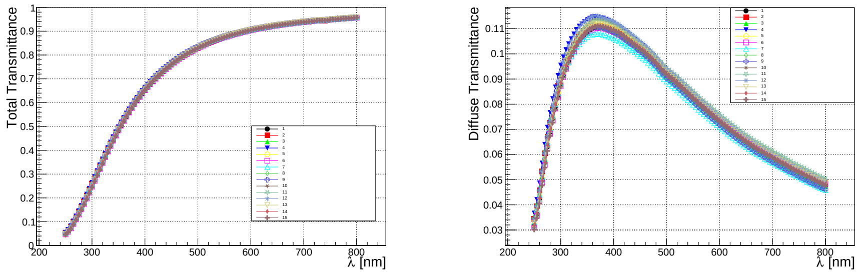

Figure 25: Total and Diffuse Transmittance sample LEC8-6

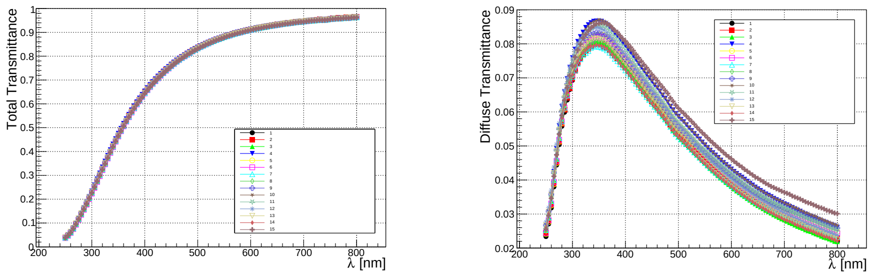

Figure 26: Total and Diffuse Transmittance sample LEC9-1

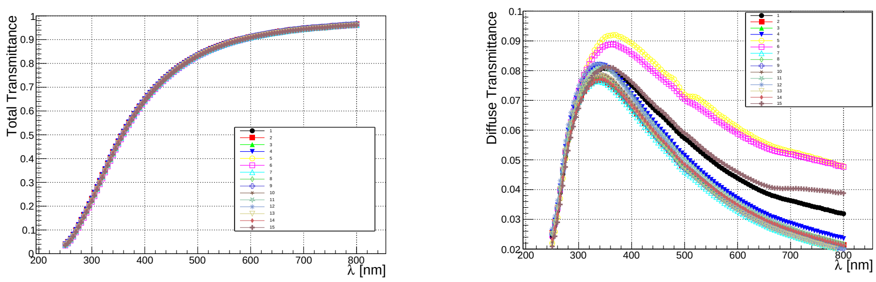

Figure 27: Total and Diffuse Transmittance sample LEC9-2

4.0.4 Transmission Length

The Transmission length (Λ_T) of a single tile was considered as the average of the transmittance value at each sampling point and was fitted by the formula described in Equation 3. The scattering and absorption are provided by the transmission length λ_T, which is a function of the absorption length λ_{abs} and scattering length λ_{scat}, as shown in this equation below. Then we assumed that the scattering length is dependent on λ^4 and the absorption length is dependent on λ^8.

$$\lambda_T = -\frac{t}{ln(T(\lambda))} \tag{3}$$

$$\lambda_{scat} = \frac{\lambda^4}{C} \tag{4}$$

$$\lambda_{abs} = \frac{\lambda^8 t}{Bt - \lambda^8 lnA} \tag{5}$$

Transmission, scattering, and absorption lengths can be extracted from the transmittance measurement, considering the parameters obtained from the fit of the transmittance curve as a function of λ according to Equation 1.

In this paper, the transmission length was extracted from linear transmittance, the difference between total and diffuse transmittance. Then, from the linear transmittance, we can define the transmission length by plotting the function in Equation 3. Normal hemispherical transmittance in the visible range was measured as well as extinction coefficients at 400 nm. These quantities are valuable parameters to quantify the image quality seen through a piece of aerogel.

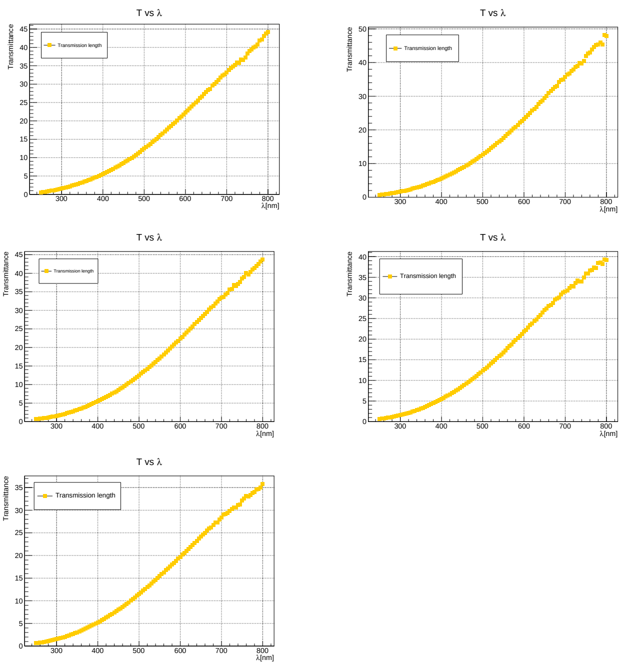

Figure 28: Transmission length of aerogel (n=1.03)

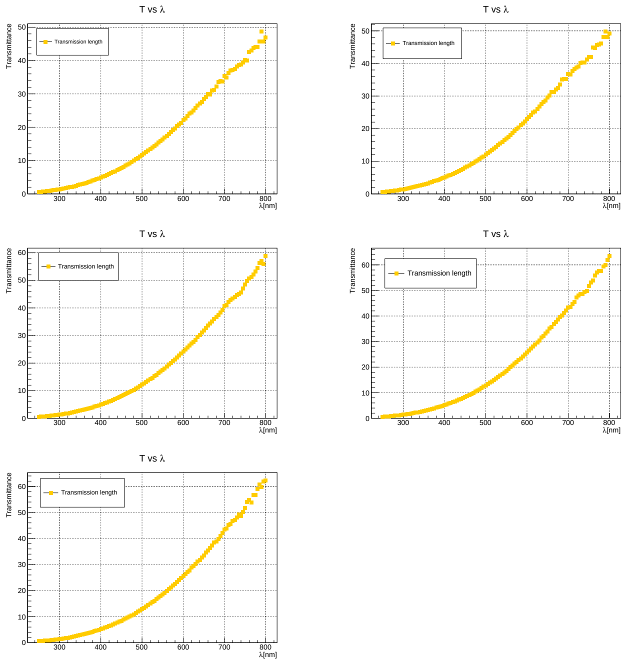

Figure 29: Transmission length of aerogel (n=1.04)

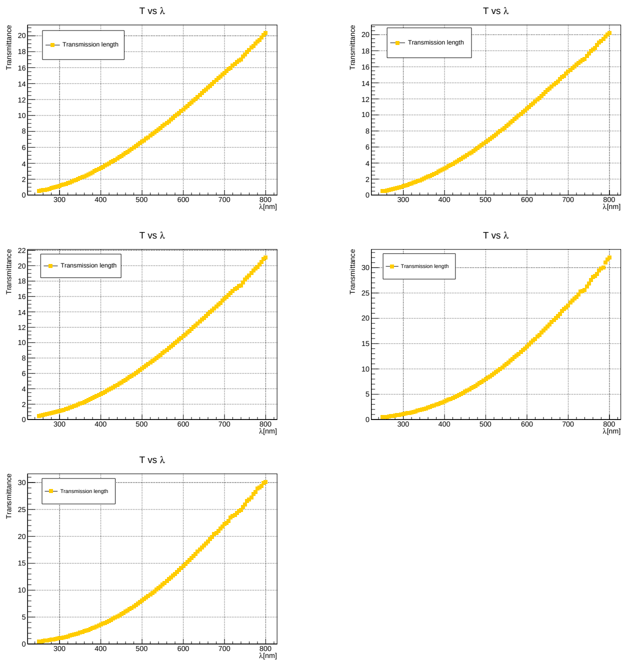

Figure 30: Transmission length of aerogel (n=1.05)

The plot of the transmission length of aerogel at each sample is shown in the figures above. The transmission length displays the expected dependency on the wavelength according to the Rayleigh scattering occurring mainly in the lower wavelength. Table 3 below shows the summary of the result related to the optical properties of all samples at wavelength 400 nm.

Table 3: Summary of the result related to the optical properties of Aerogel at 400nm

Sample	n	Transmission length
‘LEC4-2a	1.03	5.57056
LEC4-2b	1.03	5.61364
LEC6-1a	1.03	5.5095
LEC6-1b	1.03	5.49586
LEC6-2b	1.03	5.27755
LEC11-6	1.04	4.86189
LEC11-7	1.04	5.04369
LEC12-1	1.04	4.95115
LEC12-4	1.04	5.15688
LEC12-6	1.04	5.21927
LEC8-1	1.05	3.41085
LEC8-2	1.05	3.32749
LEC8-6	1.05	3.3207
LEC9-1	1.05	3.357662
LEC9-2	1.05	3.59398

Based on this table, comparing n=1.03, n=1.04, and n=1.05, the transmittance is found lowest for a very low refractive index and indicates the amount of absorption loss when light traverses a material. Conversely, the transmittance is found higher for the sample with a refractive index of n=1.03.

4.0.5 The Reflectance of Aerogel

Besides the transmittance measurement, we also provide the reflectance measurements by choosing 3 points in the middle of the aerogel's surface to measure the reflectance. The setup has been mentioned in section 3. The reflectance was measured to calculate how much is light reflected from the surface of the aerogel. Figure 28 describes the reflectance value of aerogel samples. Each sample was calculated as the average of reflectance for all 3 points. Then, the values were fitted as we can see in this figure.

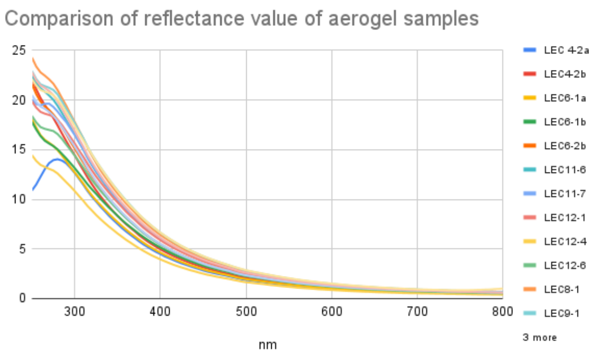

Figure 31: Reflectance value of aerogel samples

4.0.6 Silicon Photomultipliers

Silicon Photomultipliers have been photodetector technologies for detecting faint light since their development in the 1990s. SiPM offers several advantages, such as low operation voltage, compactness, ruggedness, and relatively low cost[12]. However, the Photon Detection Efficiency (ratio between the number of detected photons and the photon arriving at the detector) is still limited and rapidly decreases from the peak as the wavelength enters into ultraviolet range. This is due to reflection and Fill Factor (FF) limiting the Photo Detection Efficiency in all wavelengths. Therefore, a reduction in photon reflection at the surface plays a prominent role in the development of high-performance SiPM [14].

To reduce the photon losses due to reflection, the approach of Anti Reflection Coating (ARC) is used, because it can reduce the photon losses by making use of phase changes and the dependence of reflectivity on the refractive index. The ARC materials are thermally made from silicon dioxide and silicon nitride.

Textured surfaces with upright random nano micro pyramids can be formed by anisotropic etching. Texturing the silicon wafer surface enhances the light trapping on nano pyramidal structures of the silicon etched surface. As shown by the results, the light reflected from the planar surface is completely lost, meanwhile, the textured surface can allow the light reflected from the side of one pyramid to be reflected downward and then get a second chance to be absorbed into the silicon bulk [5].

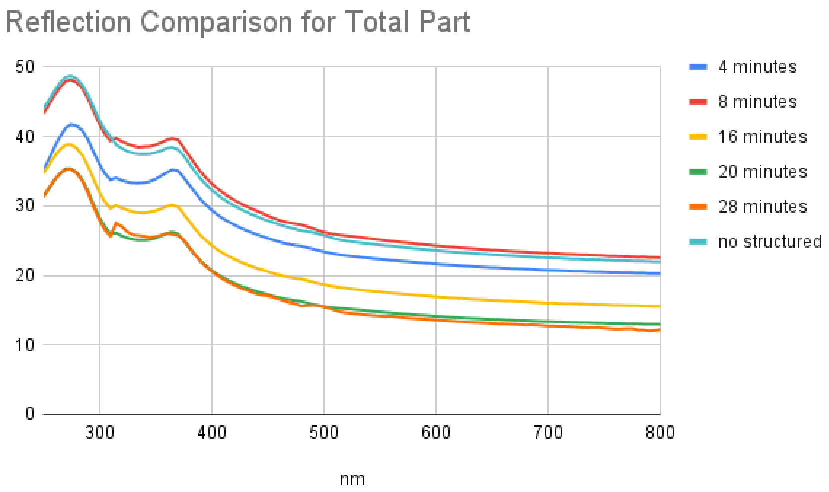

Figure 32: Reflection measurement for total part of silicon

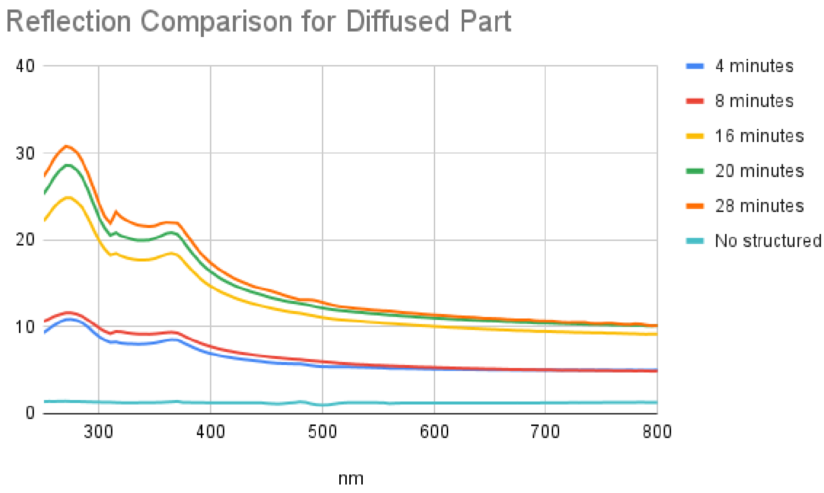

Figure 33: Reflection measurement for diffuse part of silicon

5 Conclusion

The optical characterization of aerogel in a Ring Imaging Cherenkov (RICH) detector is crucial for the performance and efficiency of the detector. Since the refractive index of the aerogel is a critical parameter that affects the Cherenkov angle and the separation of particle tracks, this paper provides the measurements of aerogel with various indexes 1.03, 1.04, 1.05.

The measurements of aerogel were performed in the UV and visible regions where Cherenkov radiation is emitted. Aerogel should be highly transparent to allow Cherenkov photons to pass through and be detected by photo-detector. The transparency depends on the transmission length of the aerogel. As shown in the result, the transmission length is found higher on the sample n=1.03 (LEC4-2b = 5.61364 at 400nm). It is indicated that the sample was effective for transmittance light in the material of aerogel. However, it has to be taken into account that the tiles show curvature towards the surface of the tile is much higher because there are some scratches on the surface of the tiles, the presence of the scratches can increase the diffused part when we plot the total and diffuse part of the measurement.

For silicon, compared to bare silicon, the longest textured silicon surface with upright nano micro-pyramids can reduce the reflection over a wide spectrum. It would be a very promising candidate for a Cherenkov photon detector in RICH Detector.

Furthermore, the scattering and absorption of the aerogel should be analyzed because the scattering of light within the aerogel can reduce the overall efficiency of the RICH Detector. The angular distribution of scattered light should also be studied to optimize the design and minimize the impact of scattering. The last thing, the optical properties of the aerogel should be homogeneous throughout the detector volume to ensure consistency of Cherenkov angle measurements. Any in-homogeneities in refractive index or density can lead to systematic errors. The aerogel's properties should also be matched with the wavelength sensitivity of the photodetector used in the RICH Detector to optimize the detection efficiency. So that the proposal of RICH Detector for ALICE 3 in Run 5 can be applied.

6 Acknowledgements

I am deeply express my gratitude to my supervisor Antonello Di Mauro. It is such a great opportunity to be part of a big project in the ALICE upgrade system for Run 5 in RICH Detector. I also would like to thank my colleagues, Anna Rita Altamura, Thomas Schneider, Miranda, Jacob Bastiaan Van Beelen, Suharyo Sumowidagdo, and Syaefudin Jaelani for helping me to measure aerogel and SiPM until finishing my project. The last, special thanks to all CERN summer students 2023 who made this summer so wonderful and amazing. Words cannot describe my happiness to work here and might come back with another opportunity.

References

[1] ALICE Collaboration. The alice experiment – a journey through qcd, 2022.

[2] ALICE Collaboration. Letter of intent for alice 3: A next-generation heavy-ion experiment at the lhc, 2022.

[3] Andreas Höpe. Chapter 6 - diffuse reflectance and transmittance. In Thomas A. Germer, Joanne C. Zwinkels, and Benjamin K. Tsai, editors, *Spectrophotometry*, volume 46 of *Experimental Methods in the Physical Sciences*, pages 179–219. Academic Press, 2014.

[4] S. Korpar, I. Adachi, H. Chagani, R. Dolenec, K. Hara, T. Iijima, P. Križan, S. Nishida, R. Pestotnik, and A. Stanovnik. Measurements of cherenkov photons with silicon photomultipliers. *Nuclear Physics B - Proceedings Supplements*, 197(1):283–287, dec 2009.

[5] S. Korpar, R. Dolenec, K. Hara, T. Iijima, P. Križan, Y. Mazuka, R. Pestotnik, A. Stanovnik, and M. Yamaoka. Silicon photomultiplier as a detector of cherenkov photons. *Nuclear Instruments and Methods in Physics Research Section A: Accelerators, Spectrometers, Detectors and Associated Equipment*, 595(1):161–164, 2008. RICH 2007.

[6] Peter Križan. Recent progress in ring imaging cherenkov counters with vacuum-based photon detectors. *Nuclear Instruments and Methods in Physics Research Section A: Accelerators, Spectrometers, Detectors and Associated Equipment*, 502(1):28–35, 2003. Experimental Techniques of Cherenkov Light Imaging. Proceedings of the Fourth International Workshop on Ring Imaging Cherenkov Detectors.

[7] MICHAEL F. L'ANNUNZIATA. 9 - cherenkov counting. In Michael F. L'Annunziata, editor, *Handbook of Radioactivity Analysis (Second Edition)*, pages 719–797. Academic Press, San Diego, second edition edition, 2003.

[8] Thibaud Mathis, Stephane Vignot, Cecila Leal, jean pierre Caujolle, C. Maschi, Martine, L. Kodjikian, Stephanie Baillif, Joel Herault, and Juliette Thariat. Mechanisms of phosphenes in irradiated patients. *Oncotarget*, 8, 07 2015.

[9] Albert Mollén and R Erlandsson. Investigation of ageing effects and image stability in hybrid photon pixel detectors at the lhcb experiment cern. 01 2010.

[10] Roman Pasechnik and Michal Šumbera. Phenomenological review on quark–gluon plasma: Concepts vs. observations. *Universe*, 3(1), 2017.

[11] Tudor E. Scheul, Edris Khorani, Tasmiat Rahman, Martin D.B. Charlton, and Stuart A. Boden. Wavelength and angle resolved reflectance measurements of pyramidal textures for crystalline silicon photovoltaics. *Progress in Photovoltaics: Research and Applications*, 28(12):1248–1257, 2020.

[12] Frank Simon. Silicon photomultipliers in particle and nuclear physics. *Nuclear Instruments and Methods in Physics Research Section A: Accelerators, Spectrometers, Detectors and Associated Equipment*, 926:85–100, 2019. Silicon Photomultipliers: Technology, Characterisation and Applications.

[13] Jiulong Sun. *Development of Inorganic-Organic Hybrid Materials for Waste Water Treatment*. PhD thesis, 12 2014.

[14] Yuguo Tao, Arith Rajapakse, and Anna Erickson. Advanced antireflection for back-illuminated silicon photomultipliers to detect faint light. *Scientific Reports*, 12, 08 2022.

[15] Wladyslaw Henryk Trzaska. New alice detectors for run 3 and 4 at the cern lhc. *Nuclear Instruments and Methods in Physics Research Section A: Accelerators, Spectrometers, Detectors and Associated Equipment*, 958:162116, 2020. Proceedings of the Vienna Conference on Instrumentation 2019.

[16] Alan A. Watson. The discovery of cherenkov radiation and its use in the detection of extensive air showers. *Nuclear Physics B - Proceedings Supplements*, 212-213:13–19, mar 2011.